

# Microstrip Circularly-Polarized Leaky-Wave Antenna with Wide Axial Ratio Bandwidth for X-Band Application

Zhongbao WANG<sup>1,2</sup>, Dezhuang ZHANG<sup>1</sup>, Mingming GAO<sup>2</sup>, Hongmei LIU<sup>1</sup>, Shaojun FANG<sup>1</sup>

<sup>1</sup>School of Information Science and Technology, Dalian Maritime University, Dalian, Liaoning 116026, China

<sup>2</sup>Liaoning Key Laboratory of Radio Frequency and Big Data for Intelligent Applications, Liaoning Technical University, Huludao, Liaoning 125105, China

wangzb@dlnu.edu.cn, zhangdz@163.com

Submitted December 26, 2023 / Accepted May 6, 2024 / Online first May 28, 2024

**Abstract.** *A microstrip circularly polarized (CP) leaky-wave antenna (LWA) operating in the X-band, and having the characteristics of a broad axial ratio bandwidth is proposed. The proposed LWA is made up of 13 unit cells in series through microstrip feeding lines. Elliptical and rectangular slots are etched in each unit cell to achieve the radiation of CP waves. The open stopband at the broadside frequency can be suppressed by shifting the feeding line position and etching two circular notches on both sides of each radiation patch. To validate the proposed method, a prototype antenna operating in the X-band is manufactured and measured. The measured result demonstrates that the  $-10$ -dB impedance bandwidth of the microstrip CP LWA is 42.2% (7.96–12.22 GHz); the 3-dB axial ratio bandwidth is 26.4% (9.2–12.2 GHz); the gain of the antenna is 16.0 dBic. Besides, the main beam maintains good CP radiation properties while it continues to scan from  $-22^\circ$  to  $+18^\circ$ .*

## Keywords

Leaky-wave antenna, circular polarization, open stopband, axial ratio bandwidth

## 1. Introduction

Leaky-wave antennas (LWAs) have drawn a lot of interest due to their high gain, low profile, and ability to vary the scanning angle of the radiation beam with frequency [1]. Various researches on LWAs have been reported, including spoof surface plasmon polariton (SSPP) transmission lines [2], substrate integrated waveguides (SIW) [3], microstrip coupled meander lines [4], and coupled pin-loaded microstrip lines [5]. However, the energy radiation of these mentioned antennas is mainly in the form of linear polarization.

Circularly polarized (CP) antennas have the characteristics of minimizing polarization mismatch, strong iono-

spheric penetration, and resistance to multipath interference, which are applied in modern wireless communication systems [6]. Several works on CP LWAs have been reported in [7–11]. The beam scanning ability of CP LWA can be generated by using horizontal and vertical slots to be etched on SIW [7]. A CP LWA through etching resembling slope slots on the half-mode substrate integrated waveguide (HMSIW) was proposed in [8], which has the characteristic of miniaturization. In [9], a multi-layer SIW CP LWA was formed by employing circular slots in the bottom layer, truncated patches in the middle layer, and H-shaped interdigital slots in the top layer. However, many metalized holes are used in CP LWAs based on SIW or HMSIW structures, resulting in low integration and high cost of antennas. Wideband CP LWA with a multi-layer structure based on the SSPP slow-wave transmission line was reported in [10]. By loading tunable varactors controlled by a single uniform DC bias voltage, the LWA is able to complete a backward-to-forward CP beam scan at a fixed frequency [11]. Unfortunately, the existence of multi-layer substrates and tunable varactor diodes increases the CP antenna's size and complexity.

Compared with the previous references [6–11], microstrip CP LWAs have the advantages of low profile and single-layer structure [12–16]. In [12], a CP leaky-wave antenna was proposed by cascading asymmetrically coupled microstrip line structure. However, it had a 3-dB axial ratio (AR) bandwidth of only 4.8%. Two orthogonal dipoles arranged on both sides of the planar Goubau line were used to generate CP beam radiation and improve the AR bandwidth of LWAs [13]. In [14], different coupled parasitic loads and meandering lines were utilized to produce CP beam scanning and increase the 3-dB AR bandwidth to 11.2%. A microstrip CP LWA with a beam-scanning angle of  $95^\circ$  was proposed in [15], which shows a 3-dB AR bandwidth of less than 12%. In [16], a broadside CP radiation microstrip LWA was presented using transversal series-fed symmetric elements. However, all the mentioned microstrip CP LWAs had narrow 3-dB AR bandwidth.

Open stopband (OSB) appears at the broadside frequency of the beam frequency scanning LWAs, which weakened the antenna's gain at the center (i.e., broadside) frequency and was caused by a mismatch of the antenna's unit cell [17]. Numerous techniques have been contributed to achieve the suppression of the OSB. Impedance matching technology with balanced conditions at the operating frequency band was used to alleviate the OSB of LWAs [18], [19]. Nevertheless, the method increases the size of antennas due to the introduction of stubs and impedance-matching networks. In [20], a rectangular slot was embedded between two adjacent unbalanced open ring resonators in the SIW unit cell, which eliminates efficiently the OSB. Besides, transversal asymmetry [21] techniques in periodic LWA were used for suppressing OSB. However, this technique requires extracting the corresponding circuit model of the LWA's unit cell, increasing the complexity of the analysis. In [22], open stubs were used to achieve asymmetric unit cells for mitigating OSB. However, the disadvantage of the adding open stub technique is that it only can suppress the OSB of microstrip linearly polarized LWA. In [16], the OSB of the CP LWA was suppressed by etching a pair of rectangular portions at the bottom corner of the patch. However, it didn't have a structure to adjust the impedance matching of the CP LWA, so the  $|S_{11}|$  of the LWA [16] had a significant increase at the broadside frequency, which implies the method in [16] has a weak OSB suppression ability. Therefore, it is necessary for microstrip CP LWA to find a simple and effective method to achieve the suppression of the OSB.

In this paper, a CP microstrip LWA with wide AR bandwidth and OSB suppression characteristics for X-band application is proposed. It has etched elliptical and rectangular slots that produce circularly polarized radiation, and the symmetrical two circular notches are etched in the radiation patch and the feeding line shifted to suppress the OSB.

## 2. Antenna Design and Analysis

### 2.1 Configuration of the Proposed CP LWA

Figure 1 shows the configuration of the proposed microstrip CP LWA with a wide AR bandwidth, which consists of thirteen cascaded unit cells. The physical dimensions of the proposed LWA  $l \times w$  is  $277 \text{ mm} \times 36 \text{ mm}$ . Two metal strips with the size of  $l_s \times w_s$  are used at two ports to achieve  $50\text{-}\Omega$  impedance matching. It is printed on a substrate with relative dielectric constant  $\epsilon_r = 2.6$  and a thickness of  $h = 1 \text{ mm}$ . The unit cell is based on a circular radiation patch. The initial radius  $r$  of the circular patch can be obtained by using the analysis formula for the fundamental mode (i.e.,  $\text{TM}_{11}$  mode) resonant frequency of the circular patch antenna [23] and making the  $\text{TM}_{11}$  mode resonant frequency less than the lowest operating frequency of the LWA. The period  $p$  of the unit cell is selected as  $\lambda_g$  at broadside frequency [24]. The evolution of the unit cell

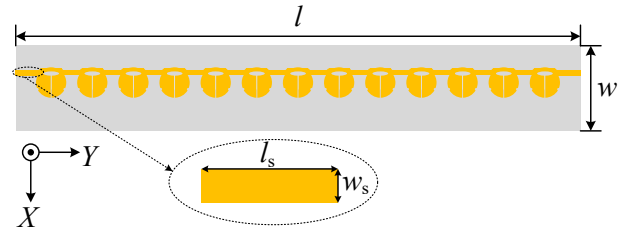


Fig. 1. The configuration of the proposed microstrip CP LWA.

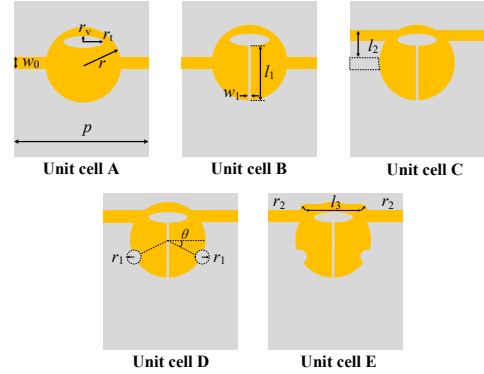


Fig. 2. The unit cell evolution from unit cell A to unit cell E.

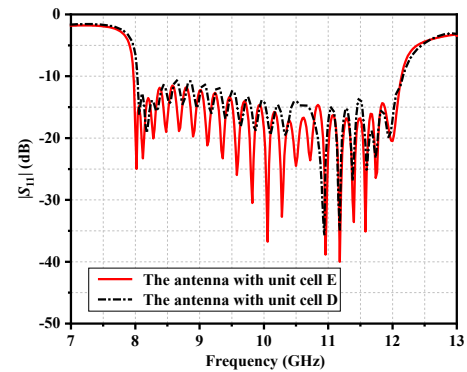


Fig. 3. The  $|S_{11}|$  of the leaky-wave antenna with the unit cell D or the unit cell E.

for the proposed microstrip CP LWA is depicted in Fig. 2. In unit cell A, a microstrip line with width  $w_0$  and a circular patch etched with an elliptical slot is employed. The  $r_v$  and  $r_1$  represent the semi-minor and semi-major axes of the etched elliptical slot, respectively. In unit cell B, a rectangular slot with the size of  $l_1 \times w_1$  is etched in the radiation patch. In unit cell C, the movement distance of the microstrip feeding line along the negative X-axis is  $l_2$ . Two circular notches with the radius of  $r_1$  are etched on both sides of the radiation patch in unit cell D. In addition, a rectangular patch with the size of  $l_3 \times r_2$  and two circular patches with the radius of  $r_2$  are added in unit cell E to reduce the impact of microstrip discontinuity and improve the impedance matching of the CP leaky-wave antenna, as shown in Fig. 3.

### 2.2 Analysis of OSB Suppression

The dispersion curve for the unit cell of the proposed CP LWA is presented in Fig. 4. The normalized phase

constant  $\beta/k_0$  and attenuation constant  $\alpha/k_0$  are shown in Fig. 4, where  $\beta$ ,  $\alpha$ , and  $k_0$  represent the phase constant of the antenna, attenuation constant, and free space wave number, respectively. The  $\beta$  and  $\alpha$  can be calculated by utilizing the formula mentioned in [25]:

$$\beta = \frac{1}{p} \left| \operatorname{Im} \left( \cosh^{-1} \left( \frac{1 - S_{11}S_{22} + S_{12}S_{21}}{2S_{21}} \right) \right) \right|, \quad (1)$$

$$\alpha = \frac{1}{p} \left| \operatorname{Re} \left( \cosh^{-1} \left( \frac{1 - S_{11}S_{22} + S_{12}S_{21}}{2S_{21}} \right) \right) \right| \quad (2)$$

where  $p$  is the period of the unit cell for the proposed CP LWA.

Figures 4(a) and 4(b) exhibit the normalized phase constants and normalized attenuation constant of five types of unit cells, respectively. As shown in Fig. 4(a), the normalized phase constant  $\beta/k_0$  of the unit cell A is less than 1 in the X-band, the unit cell A can radiate electromagnetic waves, but due to the  $\beta/k_0$  of the unit cell A constantly being greater than zero from 8 to 12 GHz, beam frequency scanning from the backward to the forward in X-band cannot be achieved. Thus, a slot with dimensions of  $w_1 \times l_1$  is etched in the radiation patch to become the unit cell B shown in Fig. 2, and then the  $\beta/k_0$  of the unit cell has zero values shown in Fig. 4(a), beam frequency scanning from the backward to the forward in X-band can be achieved.

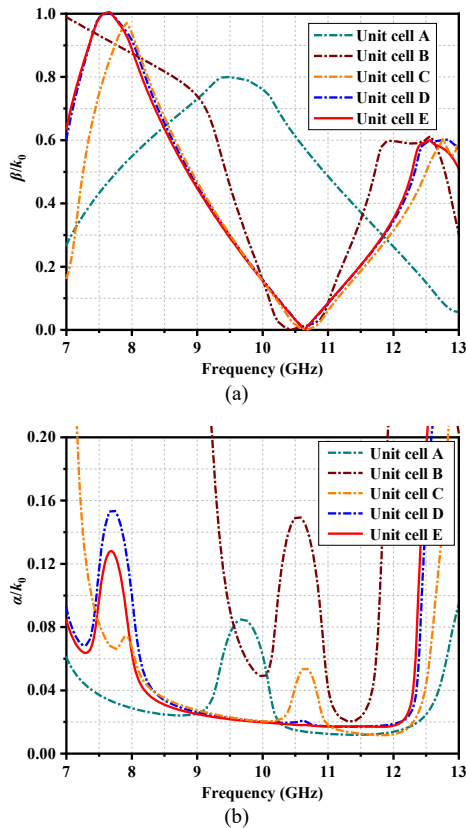


**Fig. 4.** Dispersion curves of the different unit cell. (a) Normalized phase constant. (b) Normalized attenuation constant.

However, the normalized attenuation constant  $\alpha/k_0$  of the unit cell B has significant fluctuations from 9 to 12 GHz (the fluctuation larger than 0.18, as shown in Fig. 4(b)), which implies the existence of the OSB. By shifting the feeding line from the original position at the patch center with the distance  $l_2$  (i.e., becoming the unit cell C), the fluctuation of the  $\alpha/k_0$  from 9 to 12 GHz is reduced to about 0.04 shown in Fig. 4(b). Then by adding two circular notches of radius  $r_1$  (i.e., becoming the unit cell D), the fluctuation of the  $\alpha/k_0$  from 9 to 12 GHz is further reduced. Finally, the unit cell E has a flatter  $\alpha/k_0$  from 9 to 12 GHz (as shown in Fig. 4(b)), so the OSB is suppressed and the unit cell E is used in the proposed microstrip CP LWA's design.

The azimuth  $\theta_m$  of the main beam of proposed LWA can be expressed as

$$\theta_m = \arcsin(\beta/k_0). \quad (3)$$

From (3), it is apparent that  $\theta_m$  is associated with the normalized phase constant  $\beta/k_0$ . When  $0 \leq \beta/k_0 < 1$ , the main beam of the CP LWA can gradually scan from backward to forward. On the contrary, when  $\beta/k_0 > 1$ , the electromagnetic waves of the antenna cannot radiate into free space [26].

### 2.3 Current Distribution

The simulated surface current distribution of the unit element at 10.7 GHz can be viewed in Fig. 5. It is obvious that when the microstrip CP LWA is excited with the phase being  $0^\circ$  and  $180^\circ$ , the amplitude of surface currents are almost the same, and their directions are contrary. Similarly, the same phenomenon occurs in the proposed antenna when the phases are  $90^\circ$  and  $270^\circ$ . The etched elliptical and rectangular slots cause the surface current vector at the lower part of the radiating patch to rotate clockwise at different times, which results in the proposed antenna being able to radiate the left-hand circularly polarized (LHCP) waves. Besides, the perturbation caused by the circular notches etched on both sides below the unit cell also has an undeniable impact on the CP radiation performance of the antenna.

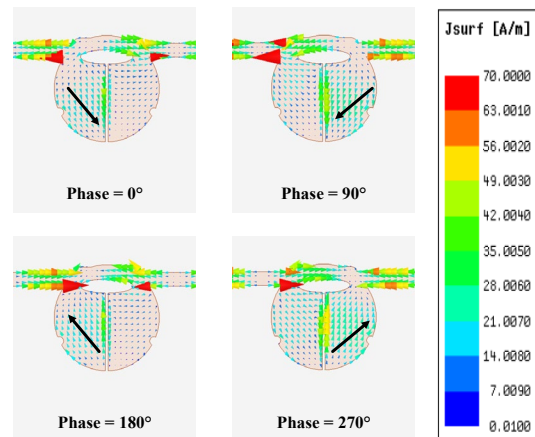


**Fig. 5.** Simulated surface current distribution of the unit cell at 10.7 GHz.

### 2.4 Optimization of Microstrip CP LWA

The effect of the semi-major axis  $r_t$  of the etched elliptical slot on the AR of the proposed CP LWA in the maximum radiation direction is shown in Fig. 6(a). It is evident that with  $r_t$  increases from 2.1 to 4.1 mm, the 3-dB AR bandwidth exhibits a trend of first increasing and then decreasing. Meanwhile, when  $r_t$  is 3.1 mm, in the (9.4 to 12.0) GHz frequency band, the simulated AR of the proposed antenna at all maximum radiation directions is less than 3 dB. From Fig. 6(b), it can be seen that when  $r_t = 3.5$  mm, the AR at 10 GHz has a minimum value of 0.5 dB, but the AR at 11 GHz is greater than 3 dB. For the AR to be less than 3 dB from 9.5 to 11 GHz, the value of  $r_t$  needs to be in the range of 2.9–3.3 mm. The effect of semi-major axis  $r_t$  on the  $|S_{11}|$  is shown in Figs. 6(c) and 6(d). It can be seen from Fig. 6(c) that as the semi-major axis  $r_t$  of the etched elliptical slot increases from 2.1 to 3.1 mm, the impedance bandwidth for  $|S_{11}| < -10$  dB increases from 40.2% to 41.0%. When  $r_t$  is 4.1 mm, the  $|S_{11}|$  at 10.7 GHz is greater than  $-7.4$  dB, which means that the OSB effect of the antenna is not suppressed. Figure 6(d) illustrates that when  $r_t$  is increased from 2.9 to 3.3 mm, the  $|S_{11}|$  for all four frequencies is less than  $-14.5$  dB, and the  $|S_{11}|$  at 11 GHz has a minimum value of  $-18.5$  dB at  $r_t = 3.1$  mm. Thus, after taking into account the AR, OSB suppression capabilities, and  $|S_{11}|$ ,  $r_t$  is finally determined to be 3.1 mm.

Figures 7(a) and 7(b) give the effect of the semi-minor axis  $r_v$  variation of the etched elliptical slot on the AR of the proposed CP LWA in the maximum radiation direction. As presented in Fig. 7(a), as  $r_v$  increases from 0.43 to 1.23 mm, the AR of the CP antenna at 10.7 GHz firstly reduces from 5.0 to 1.5 dB and then increases from 1.5 to 6.5 dB. Figure 7(b) shows that as  $r_v$  increases from 0.23 to 1.43 mm, the AR at 10.5 and 11.0 GHz firstly decreases and subsequently increases. The AR curves for 10.5 and 11.0 GHz intersect at the  $r_v$  of about 0.86 mm with an AR of 1.7 dB. In addition, as the  $r_v$  increases from 0.73 to 0.93 mm, the AR at 9.5 GHz gradually increases. It is obvious from Fig. 7(c) that the  $|S_{11}|$  is greater than  $-10$  dB from 10.54 to 10.96 GHz when the  $r_v$  is 1.23 mm. The impedance mismatch in the broadside frequency is caused by the OSB effect [17]. As shown in Fig. 7(d), when  $r_v = 0.83$  mm, the  $|S_{11}|$  for all four frequencies is less than  $-14$  dB. To accomplish the proposed CP LWA's circular polarization and the OSB suppression requirements and work in the X-band,  $r_v$  is selected as 0.83 mm.

The effect of the etched circular notch radius  $r_1$  on the AR and  $|S_{11}|$  of the proposed antenna is introduced in Fig. 8. As shown in Fig. 8(a), when the radius  $r_1$  increases from 0.1 to 0.9 mm, the 3-dB AR bandwidth of the antenna decreases from 24.2% to 11.4%. It can be seen from Fig. 8(b) that as  $r_1$  increases from 0.3 to 0.9 mm, the AR at 10 and 11 GHz decreases, but the AR at 10.5 GHz increases (especially when  $r_1$  is greater than 0.5 mm). As shown in Fig. 8(c), when  $r_1$  increases from 0.1 to 0.9 mm,  $|S_{11}|$  at 10.7 GHz increases from  $-25.6$  to  $-11.5$  dB. Figure 8(d) shows that as  $r_1$  increases from 0.5 to 0.9 mm,  $|S_{11}|$

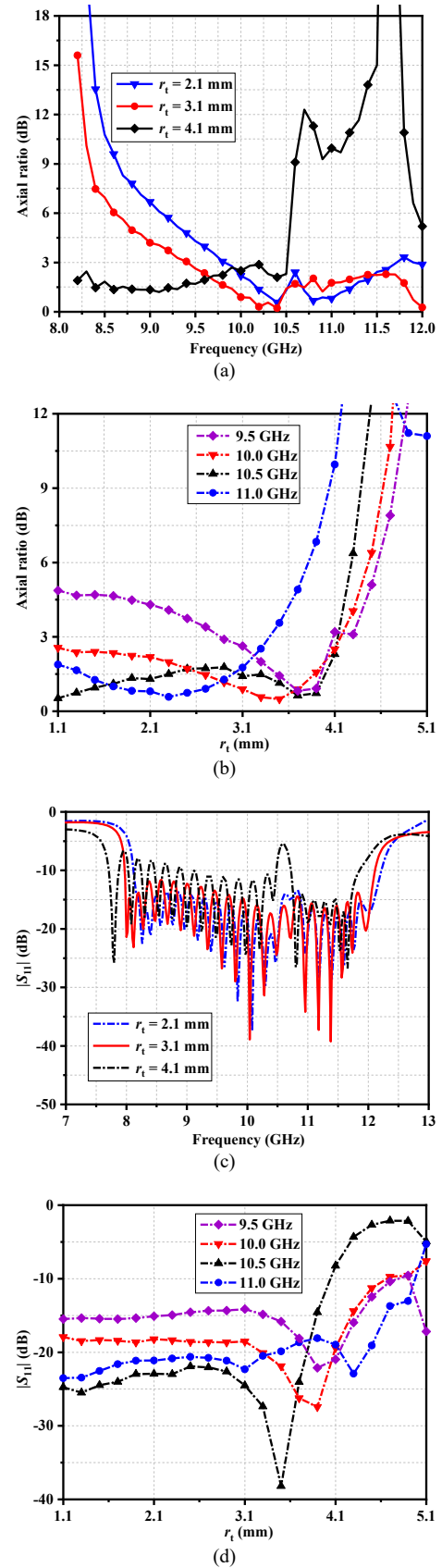


**Fig. 6.** Effect of  $r_t$  on the AR and  $|S_{11}|$  of the proposed microstrip CP LWA with  $r_v = 0.83$  mm,  $r_1 = 0.5$  mm,  $\theta = 26^\circ$ , and  $w_1 = 0.35$  mm. (a) AR versus frequency. (b) AR versus  $r_t$ . (c)  $|S_{11}|$  versus frequency. (d)  $|S_{11}|$  versus  $r_t$ .

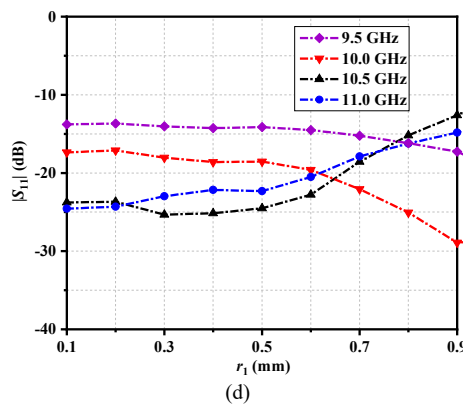
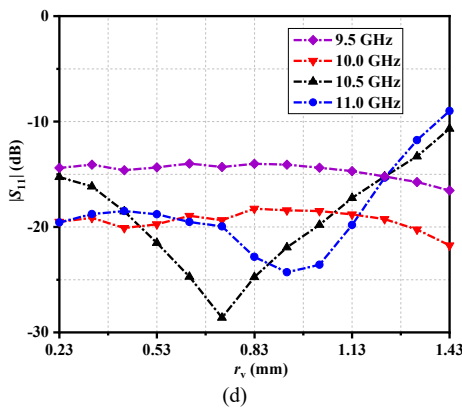
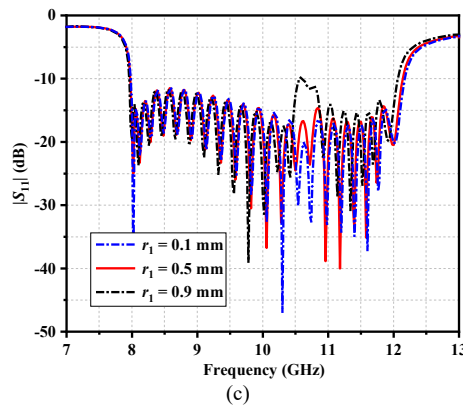
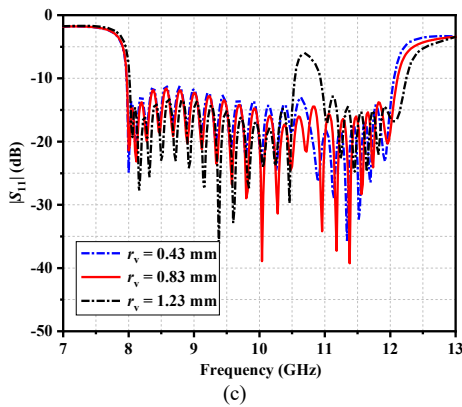
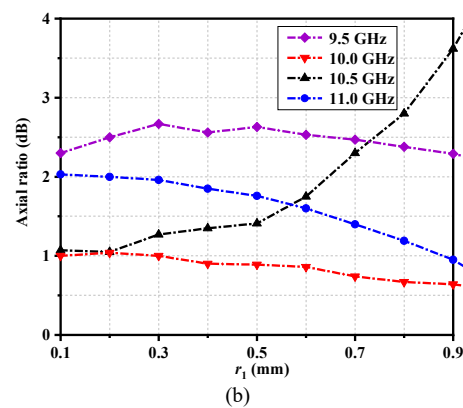
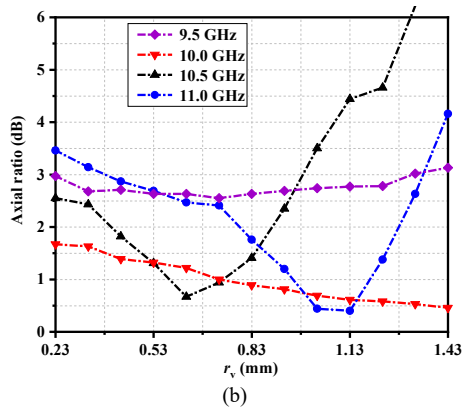
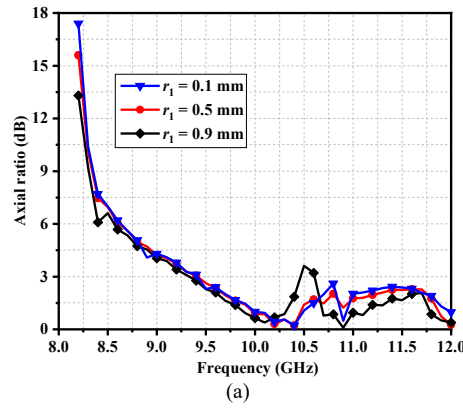
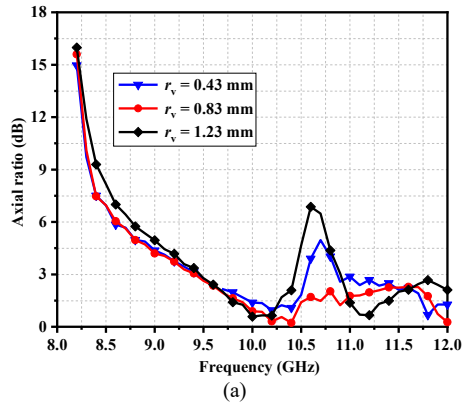


**Fig. 7.** Effect of  $r_v$  on the AR and  $|S_{11}|$  of the proposed microstrip CP LWA with  $r_t = 3.1$  mm,  $r_1 = 0.5$  mm,  $\theta = 26^\circ$ , and  $w_1 = 0.35$  mm. (a) AR versus frequency. (b) AR versus  $r_v$ . (c)  $|S_{11}|$  versus frequency. (d)  $|S_{11}|$  versus  $r_v$ .

**Fig. 8.** Effect of  $r_1$  on the AR and  $|S_{11}|$  of the proposed microstrip CP LWA with  $r_t = 3.1$  mm,  $r_v = 0.83$  mm,  $\theta = 26^\circ$ , and  $w_1 = 0.35$  mm. (a) AR versus frequency. (b) AR versus  $r_1$ . (c)  $|S_{11}|$  versus frequency. (d)  $|S_{11}|$  versus  $r_1$ .

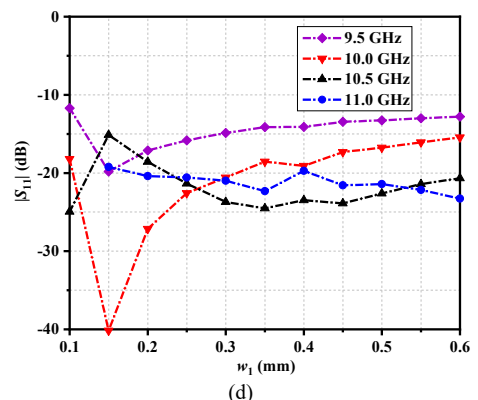
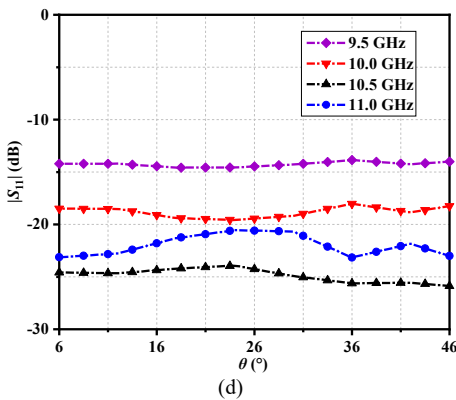
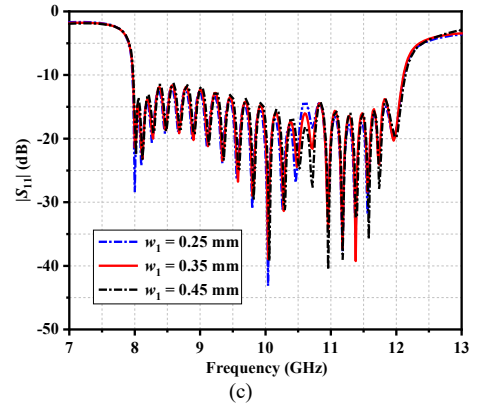
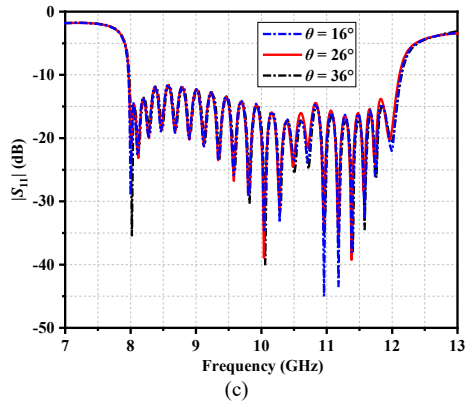
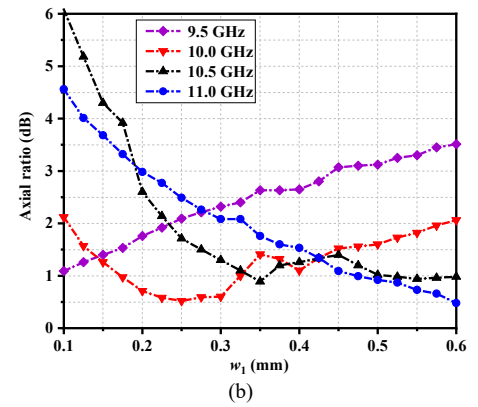
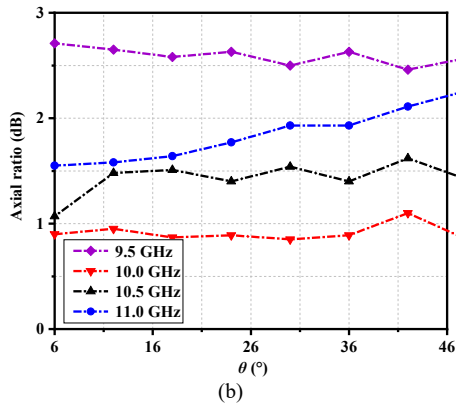
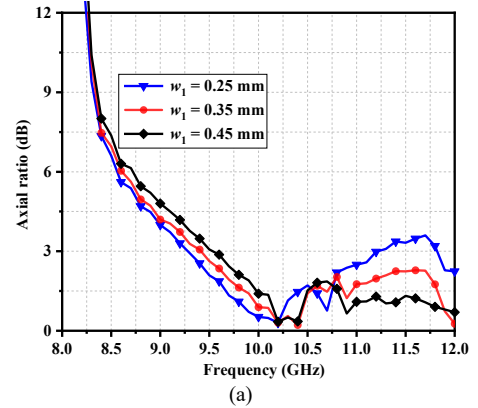
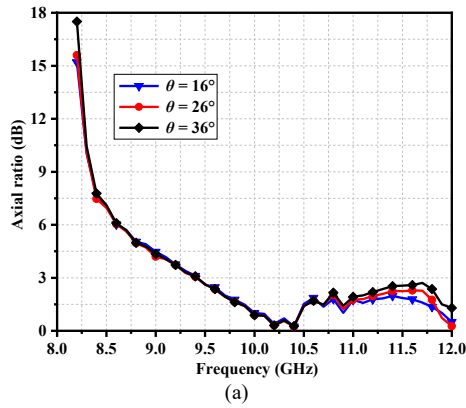


**Fig. 9.** Effect of  $\theta$  on the AR and  $|S_{11}|$  of the proposed microstrip CP LWA with  $r_t = 3.1$  mm,  $r_v = 0.83$  mm,  $r_1 = 0.5$  mm, and  $w_1 = 0.35$  mm. (a) AR versus frequency. (b) AR versus  $\theta$ . (c)  $|S_{11}|$  versus frequency. (d)  $|S_{11}|$  versus  $\theta$ .

**Fig. 10.** Effect of  $w_1$  on the AR and  $|S_{11}|$  of the proposed microstrip CP LWA with  $r_t = 3.1$  mm,  $r_v = 0.83$  mm,  $r_1 = 0.5$  mm, and  $\theta = 26^\circ$ . (a) AR versus frequency. (b) AR versus  $w_1$ . (c)  $|S_{11}|$  versus frequency. (d)  $|S_{11}|$  versus  $w_1$ .

at 10.5 and 11.0 GHz gradually increase. Figures 8(c) and 8(d) indicate that the OSB suppression ability of the microstrip CP LWA is deteriorating with the increase of  $r_1$  from 0.5 to 0.9 mm. Overall, considering the AR and  $|S_{11}|$  performances,  $r_1$  is ultimately chosen as 0.5 mm.

Figure 9 gives the effect of the rotating angle  $\theta$  of two circular notches etched on both sides of the radiation patch on the AR and  $|S_{11}|$ . It can be seen from Fig. 9(a) that  $\theta$  can be used to improve the AR performance at the upper band from 11.0 to 12.0 GHz. As shown in Fig. 9(b), the AR for all four frequencies always is less than 2.4 dB with the increase of  $\theta$  from  $6^\circ$  to  $46^\circ$ . When  $\theta = 26^\circ$ , the AR of the antenna at 10.0 GHz is 0.9 dB. It can be seen from Fig. 9(d) that as  $\theta$  increases from  $16^\circ$  to  $26^\circ$ ,  $|S_{11}|$  for all four frequencies always is less than  $-14.5$  dB. To obtain good AR bandwidth, the rotation angle  $\theta$  is set as  $26^\circ$ .

The variation of AR versus frequency and slot width  $w_1$  are given in Figs. 10(a) and 10(b), respectively. Figure 10(a) shows that the antenna's 3-dB AR bandwidth rises from 19.3% to 24.2% as  $w_1$  increases from 0.25 to 0.35 mm. Figure 10(b) demonstrates that there is an opposing trend in AR at 9.5 and 11 GHz when  $w_1$  increases from 0.1 to 0.6 mm. And when  $w_1$  is in the range from 0.2 to 0.44 mm, the AR for all four frequencies is less than 3 dB. As shown in Fig. 10(c), the increase of  $w_1$  from 0.25 to 0.45 mm has a relatively small effect on the  $|S_{11}|$ . It can be seen from Fig. 10(d) that as  $w_1$  increases from 0.2 to 0.44 mm, the  $|S_{11}|$  at 9.5 and 10 GHz gradually increases, but both are less than  $-13$  dB. At 10.5 GHz, the  $|S_{11}|$  of the antenna has a minimum value of  $-24.5$  dB when  $w_1 = 0.35$  mm. After taking into account the antenna's 3-dB AR bandwidth and  $|S_{11}|$ ,  $w_1$  is determined to be 0.35 mm.

Figure 11 gives the effect of the number of unit cells on the gain of the proposed microstrip CP LWA at 10.7 GHz. It can be seen from Fig. 11 that as the number of unit cells increases from 9 to 16, the gain of the proposed microstrip CP LWA increases from 13.68 to 16.95 dBic. To design a leaky-wave antenna with a gain larger than 15.5 dBic, the number of unit cells is selected as 13. Meanwhile, by Ansys HFSS simulation, the proposed microstrip CP LWA's final dimensions have been identified and presented in Tab. 1.

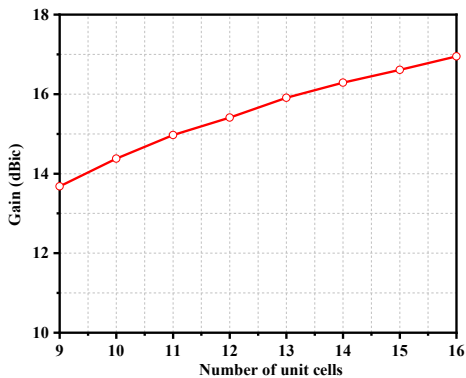


Fig. 11. Effect of the number of unit cells on the gain of the proposed microstrip CP LWA at 10.7 GHz.

$l$	$l_s$	$l_1$	$l_2$	$l_3$	$w$	$w_s$
277	16.7	9.1	4.5	6.1	36	2.5
$w_1$	$p$	$r$	$r_v$	$r_t$	$r_1$	$r_2$
0.35	19.5	6.2	0.83	3.1	0.5	0.6

Tab. 1. Dimensions of the proposed microstrip CP LWA. (unit: mm).

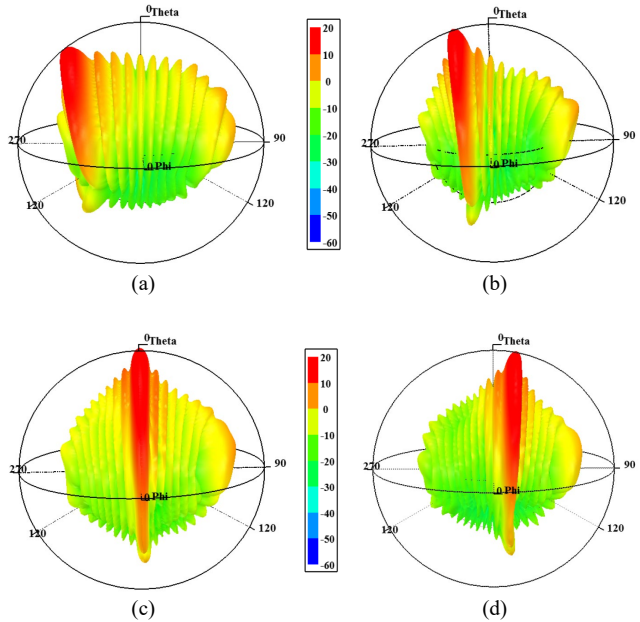


Fig. 12. Simulated 3D radiation patterns of the proposed microstrip CP LWA: (a) 8.5 GHz, (b) 9.5 GHz, (c) 10.7 GHz, (d) 11.5 GHz.

Figure 12 gives the simulated 3D radiation patterns of the proposed microstrip CP LWA. It can be seen that as the frequency increases from 8.5 to 11.5 GHz, the main beam of the proposed leaky-wave antenna scans from backward to forward, and the broadside radiation frequency is 10.7 GHz.

### 3. Simulated and Measured Results

Figure 13 provides a photograph of the manufactured microstrip CP LWA. The far-field performances of the manufactured LWA are measured in the microwave anechoic chamber, and the  $S$ -parameters are measured using an Agilent N5230A vector network analyzer. Figure 14 shows the simulated and measured  $S$ -parameters of the proposed CP antenna. As seen in Fig. 14, the measured



Fig. 13. Photograph of the manufactured microstrip CP LWA. (a) Top layer. (b) Bottom layer.

reflection coefficient  $|S_{11}|$  is less than  $-10$  dB, and transmission coefficient  $|S_{21}|$  is less than  $-7.3$  dB from 7.96 to 12.22 GHz. Moreover, the measured  $|S_{11}|$  is  $-15.2$  dB at the broadside frequency of 10.7 GHz, indicating that OSB is effectively suppressed. Figure 15 gives the simulated and measured normalized radiation pattern of the proposed microstrip CP LWA. The measured results demonstrate that the proposed antenna is capable of a main-beam scanning range of  $-52^\circ$  to  $+18^\circ$  in the frequency range from 8.2 to 12.0 GHz. The sidelobe level of the proposed microstrip CP LWA is below  $-11$  dB at all frequencies from 8.2 to 12 GHz. The AR and gain curves for simulation and measurement are shown in Fig. 16. The measured 3-dB AR bandwidth is 26.4% from 9.2 to 12.0 GHz. In the 3-dB AR bandwidth, the measured gain is more than 11.2 dBic with a maximum gain value of 16.0 dBic. The simulated and measured main beam-scanning angle of the proposed microstrip CP LWA is shown in Fig. 17. It can be seen that the measured main beam-scanning angle is from  $-24^\circ$  to  $+18^\circ$  within the 3-dB AR bandwidth (i.e., 9.2–12.0 GHz). The first reason for the differences between the simulated and measured results is the tolerance of the substrate dielectric constant and the fabricated LWA prototype. Among them, the nominal deviation of the permittivity of the used substrate is  $\pm 0.05$  when leaving the factory, and the nominal deviation during the antenna manufacturing process is  $\pm 0.1$  mm. The second reason is the measurement tolerance of the far-field measurement system in the microwave anechoic chamber.

The comparisons between the proposed LWA and existing antennas are provided in Tab. 2. It reveals that the AR bandwidth of the proposed LWA is 26.4%, which is wider than [9], [12–14] and [16]. Furthermore, compared to existing antennas, wider impedance bandwidth, higher gain, and simpler structure can be accomplished using the proposed microstrip LWA in the X-band.

### 4. Conclusion

In this paper, a microstrip CP LWA with wide impedance bandwidth and AR bandwidth is proposed for X-band application. The characteristics of CP radiation and OSB suppression have been achieved by etching slots of different shapes in the circular radiation patch. Specifically, adjusting the movement distance  $l_2$  of the feeding microstrip line can significantly suppress the OSB, and etching two circular notches with the radius of  $r_1$  can also further suppress the OSB. In accordance with the measurement results, the main beam of the proposed antenna can scan from  $-52^\circ$  to  $+18^\circ$  in the impedance bandwidth from 7.96 to 12.22 GHz, and the 3-dB AR bandwidth is 26.4% from 9.2 to 12.0 GHz with a maximum gain of 16.0 dBic. Compared with the existing CP LWAs [9], [12–14], [16], the radiation performances of the proposed CP LWA have been significantly enhanced by using the proposed unit cell in this paper. Therefore, due to its superior performance in wide impedance and AR bandwidth,

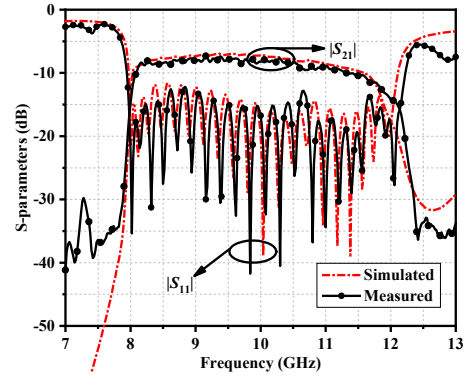


Fig. 14. Simulated and measured results of S-parameters for the proposed microstrip CP LWA.

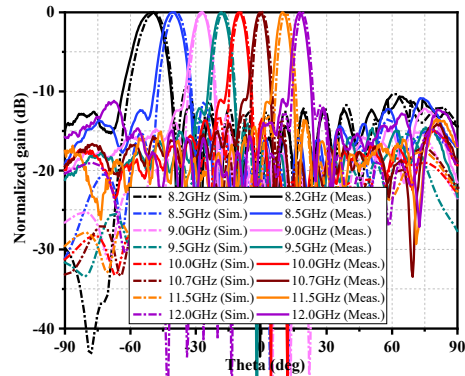


Fig. 15. Simulated and measured results of normalized radiation pattern for the proposed microstrip CP LWA.

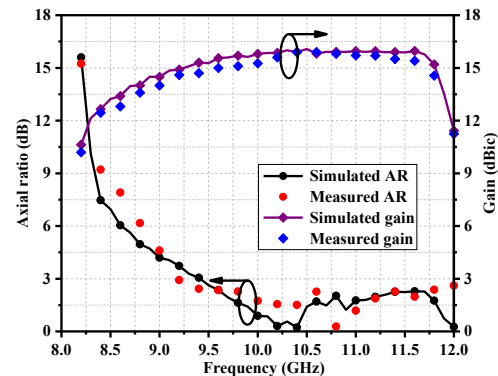


Fig. 16. Simulated and measured results of the gain and AR for the proposed microstrip CP LWA.

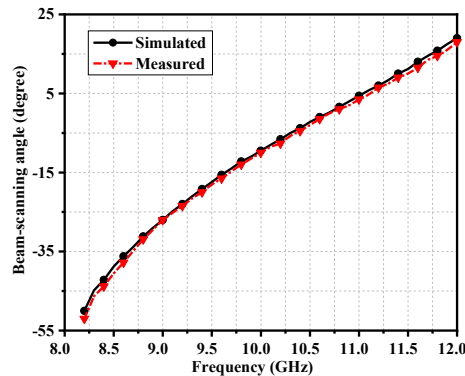


Fig. 17. Simulated and measured the main beam-scanning angle of the proposed microstrip CP LWA.

Refs.	Antenna type	$ S_{11}  < -10$ dB BW (%)	AR < 3 dB BW (%)	Polarization mode	Scan angle	Gain
[9]	SIW	7.62–10.67 GHz (33.1%)	8.3–10.6 GHz (24.3%)	CP	−38° to +71°	10.5 dBic
[12]	Meandering microstrip	8.1–8.5 GHz (4.8%)	8.10–8.50 GHz (4.8%)	CP	−31° to +6°	9.1 dBic
[13]	Planar Goubau line	36.0–42.0 GHz (15.0%)	38.0–41.0 GHz (7.6%)	CP	−19.6° to −17.5°	15.6 dBic
[14]	Coupling microstrip	9.7–11.7 GHz (26.1%)	10.1–11.4 GHz (11.2%)	CP	−4° to +18°	12.7 dBic
[16]	Periodic microstrip	7.5–11.7 GHz (43.0%)	9.1–10.4 GHz (13.3%)	CP	−48° to +16°	15.8 dBic
[22]	Meandering microstrip	6.0–7.3 GHz (19.6%)	-	LP	−60° to +58°	12.6 dBi
Proposed antenna	Periodic microstrip	7.96–12.22 GHz (42.2%)	9.2–12.0 GHz (26.4%)	CP	−52° to +18°	16.0 dBic

**Tab. 2.** Comparisons of the proposed LWA with existing antennas.

high gain, and continuous beam scanning, radar and X-band satellite communication are two areas where the proposed antenna has significant potential for use.

## Acknowledgments

This work was supported by the National Natural Science Foundation of China (No. 61871417), the Liaoning Revitalization Talents Program (No. XLYC2007024), the Fundamental Research Funds for the Central Universities (No. 3132023243), and the Open Fund of Liaoning Key Laboratory of Radio Frequency and Big Data for Intelligent Applications.

## References

- [1] JACKSON, D. R., CALOZ, C., ITOH, T. Leaky-wave antennas. *Proceedings of the IEEE*, 2012, vol. 100, no. 7, p. 2194–2206. DOI: 10.1109/JPROC.2012.2187410
- [2] JIDI, L., CAO, X., GAO, J., et al. Ultrawide-angle and high-scanning-rate leaky wave antenna based on spoof surface plasmon polaritons. *IEEE Transactions on Antennas and Propagation*, 2022, vol. 70, no. 3, p. 2312–2317. DOI: 10.1109/TAP.2021.3111182
- [3] LIU, J., JACKSON, D. R., LONG, Y. Substrate integrated waveguide (SIW) leaky-wave antenna with transverse slots. *IEEE Transactions on Antennas and Propagation*, 2012, vol. 60, no. 1, p. 20–29. DOI: 10.1109/TAP.2011.2167910
- [4] WANG, H., SUN, S., XUE, X. A periodic meandering microstrip line leaky-wave antenna with consistent gain and wide-angle beam scanning. *International Journal of RF and Microwave Computer-Aided Engineering*, 2022, vol. 32, no. 7, p. 1–9. DOI: 10.1002/mmce.23162
- [5] DUAN, J., ZHU, L. A transversal single-beam  $\text{EH}_0$ -mode microstrip leaky-wave antenna on coupled microstrip lines under differential operation. *IEEE Antennas and Wireless Propagation Letters*, 2021, vol. 20, no. 4, p. 592–596. DOI: 10.1109/LAWP.2021.3058277
- [6] HAN, M., DOU, W. Compact clock-shaped broadband circularly polarized antenna based on characteristic mode analysis. *IEEE Access*, 2019, vol. 7, p. 159952–159959. DOI: 10.1109/ACCESS.2019.2951371
- [7] LYU, Y.-L., MENG, F.-Y., YANG, G.-H., et al. Periodic SIW leaky-wave antenna with large circularly polarized beam scanning range. *IEEE Antennas and Wireless Propagation Letters*, 2017, vol. 16, p. 2493–2496. DOI: 10.1109/LAWP.2017.2726089
- [8] SAGHATI, A. P., MIRSALEHI, M. M., NESHATI, M. H. A HMSIW circularly polarized leaky-wave antenna with backward, broadside, and forward radiation. *IEEE Antennas and Wireless Propagation Letters*, 2014, vol. 13, p. 451–454. DOI: 10.1109/LAWP.2014.2309557
- [9] AGARWAL, R., YADAVA, R. L., DAS, S. A multilayered SIW-based circularly polarized CRLH leaky wave antenna. *IEEE Transactions on Antennas and Propagation*, 2021, vol. 69, no. 10, p. 6312–6321. DOI: 10.1109/TAP.2021.3082618
- [10] GUAN, D.-F., YOU, P., ZHANG, Q., et al. A wide-angle and circularly polarized beam-scanning antenna based on microstrip spoof surface plasmon polariton transmission line. *IEEE Antennas and Wireless Propagation Letters*, 2017, vol. 16, p. 2538–2541. DOI: 10.1109/LAWP.2017.2731877
- [11] FU, J.-H., LI, A., CHEN, W., et al. An electrically controlled CRLH-inspired circularly polarized leaky-wave antenna. *IEEE Antennas and Wireless Propagation Letters*, 2017, vol. 16, p. 760 to 763. DOI: 10.1109/LAWP.2016.2601960
- [12] XU, S.-D., GUAN, D.-F., LIU, L., et al. A narrow-band circularly polarized leaky-wave antenna with open stopband suppressed. *International Journal of RF and Microwave Computer-Aided Engineering*, 2021, vol. 31, no. 7, p. 1–7. DOI: 10.1002/mmce.22647
- [13] SÁNCHEZ-ESCUDEROS, D., FERRANDO-BATALLER, M., HERRANZ, J. I., et al. Low-loss circularly polarized periodic leaky-wave antenna. *IEEE Antennas and Wireless Propagation Letters*, 2015, vol. 15, p. 614–617. DOI: 10.1109/LAWP.2015.2463672
- [14] ZHAO, S., DONG, Y. Circularly polarized beam-steering microstrip leaky-wave antenna based on coplanar polarizers. *IEEE Antennas and Wireless Propagation Letters*, 2022, vol. 21, no. 11, p. 2259–2263. DOI: 10.1109/LAWP.2022.3202688
- [15] RAHMANI, M. H., DESLANDES, D. Backward to forward scanning periodic leaky-wave antenna with wide scanning range. *IEEE Transactions on Antennas and Propagation*, 2017, vol. 65, no. 7, p. 3326–3335. DOI: 10.1109/TAP.2017.2705021

- [16] AHMAD, A., MUKHERJEE, J. Microstrip leaky-wave antenna with circular polarization and broadside radiation. *IEEE Antennas and Wireless Propagation Letters*, 2023, vol. 22, no. 9, p. 2265 to 2269. DOI: 10.1109/LAWP.2023.3283398
- [17] NI, H., GU, X., WU, K., et al. Compact SIW leaky-wave antenna with open-stopband suppression. *IEEE Antennas and Wireless Propagation Letters*, 2023, vol. 10, p. 2467–2471. DOI: 10.1109/LAWP.2023.3291390
- [18] PAULOTTO, S., BACCARELLI, P., FREZZA, F., et al. A novel technique for open-stopband suppression in 1-D periodic printed leaky-wave antennas. *IEEE Transactions on Antennas and Propagation*, 2009, vol. 57, no. 7, p. 1894–1906. DOI: 10.1109/TAP.2009.2019900
- [19] ZHANG, P. F., ZHU, L., SUN, S. Microstrip-line EH1/EH2-mode leaky-wave antennas with backward-to-forward scanning. *IEEE Antennas and Wireless Propagation Letters*, 2020, vol. 19, no. 12, p. 2363–2367. DOI: 10.1109/LAWP.2020.3033064
- [20] XU, K., WANG, Q., LV, L., et al. SIW-based-band leaky-wave antenna with improved beam steering performance. *IEEE Antennas and Wireless Propagation Letters*, 2022, vol. 21, no. 11, p. 2224 to 2228. DOI: 10.1109/LAWP.2022.3195215
- [21] OTTO, S., CHEN, Z., AL-BASSAM, A., et al. Circular polarization of periodic leaky-wave antennas with axial asymmetry: Theoretical proof and experimental demonstration. *IEEE Transactions on Antennas and Propagation*, 2014, vol. 62, no. 4, p. 1817–1829. DOI: 10.1109/TAP.2013.2297169
- [22] JIANG, H., XU, K., ZHANG, Q., et al. Backward-to-forward wide-angle fast beam-scanning leaky-wave antenna with consistent gain. *IEEE Transactions on Antennas and Propagation*, 2021, vol. 69, no. 5, p. 2987–2992. DOI: 10.1109/TAP.2020.3029721
- [23] DAHELE, J., LEE, K. Effect of substrate thickness on the performance of a circular-disk microstrip antenna. *IEEE Transactions on Antennas and Propagation*, 1983, vol. 31, no. 2, p. 358–360. DOI: 10.1109/TAP.1983.1143037
- [24] WANG, H., SUN, S., XUE, X., et al. A periodic coplanar strips leaky-wave antenna with horizontal wide-angle beam scanning and stable radiation. *IEEE Transactions on Antennas and Propagation*, 2022, vol. 70, no. 10, p. 9861–9866. DOI: 10.1109/TAP.2022.3177514
- [25] SARKAR, A., PHAM, D. A., LIM, S. Tunable higher order mode-based dual-beam CRLH microstrip leaky-wave antenna for V-band backward-broadside-forward radiation coverage. *IEEE Transactions on Antennas and Propagation*, 2020, vol. 68, no. 10, p. 6912–6922. DOI: 10.1109/TAP.2020.2995300
- [26] SUN, L., HOU, Y., LI, Y., et al. An open cavity leaky-wave antenna with vertical-polarization endfire radiation. *IEEE*

*Transactions on Antennas and Propagation*, 2019, vol. 67, no. 5, p. 3455–3460. DOI: 10.1109/TAP.2019.2902662

## About the Authors ...

**Zhongbao WANG** received the Ph.D. degree in Communication and Information Systems from Dalian Maritime University (DMU), China, in 2012. He is currently a Full Professor with the School of Information Science and Technology, DMU. From 2014 to 2018, he was a Postdoctoral Fellow with Beijing University of Posts and Telecommunications, China. From 2019 to 2020, he was a Visiting Scholar with the National University of Singapore, Singapore. He has authored more than 80 journal papers. He is currently serving as a Technical Reviewer for the IEEE Transactions on Circuits and Systems, MTT, MWTL, Radioengineering, and so on. His current research interests include balanced RF components and CP antennas.

**Dezhuang ZHANG** was born in Jining, Shandong, China. He is currently working toward the M.Eng. degree in Communication Engineering at DMU. His current research interests focus on microstrip leaky wave antenna.

**Mingming GAO** received the Ph.D. degree in 2015. She is currently an Associate Professor with Liaoning Technical University. Her main research interests include RF circuit and antenna.

**Hongmei LIU** received the Ph.D. degree in Communication and Information Systems from DMU, China, in 2016. She is currently an Associate Professor with the School of Information Science and Technology, DMU. Her current research interests include passive microwave circuits, reconfigurable RF components, and CP microwave antennas.

**Shaojun FANG** received the Ph.D. degree in Communication and Information Systems from DMU, China, in 2001. Since 1982, he has been at DMU, where he is currently the Head Professor with the School of Information Science and Technology. His recent research interests include passive RF components and antennas.